# Virtual Flight Demonstration of the Stratospheric Dual-Aircraft Platform

## NIAC Phase I Final Report

W. A. Engblom, PI %
Embry-Riddle Aeronautical University

Contributors:
R. K. Decker/NASA, H. Y. Moncayo/ERAU, W. C. Barott/ERAU,
E. L. Sanchez/ERAU, A. A. Giovagnoli/ERAU

March 9, 2016

# Executive Summary

A baseline configuration for the dual-aircraft platform (DAP) concept is described and evaluated in a physics-based flight dynamics simulations for two month-long missions as a communications relay in the lower stratosphere above central Florida, within 150-miles of downtown Orlando.

The DAP configuration features two large glider-like (130 ft wing span) unmanned aerial vehicles connected via a long adjustable cable (total extendible length of 3000 ft) which effectively *sail* without propulsion using available wind shear. Use of onboard LiDAR wind profilers to *forecast* wind distributions are found to be necessary to enable the platform to efficiently adjust flight conditions to remain sailing by finding sufficient wind shear across the platform. The aircraft derive power from solar cells, like a conventional solar aircraft, but also extract wind power using the propeller as a turbine when there is an excess of wind shear available.

Month-long atmospheric profiles (at 3-5 min intervals) in the vicinity of 60,000-ft are derived from archived data measured by the 50-Mhz Doppler Radar Wind Profiler at Cape Canaveral and used in the DAP flight simulations. A cursory evaluation of these datasets show that sufficient wind shear for DAP sailing is persistent, suggesting that DAP could potentially sail over 90% of the month-long durations even when limited by modest ascent/descent rates.

DAP's novel guidance software uses a non-linear constrained optimization technique to define *waypoints* such that sailing mode of flight is maintained where possible, and minimal thrust is required where sailing is not practical. A set of constraints are identified which result in waypoints that enable efficient flight (i.e., minimal use of propulsion) over the two month-long flight simulations. Waypoint solutions may need to be tabulated for a wide range of potential atmospheric conditions and stored onboard for quick retrieval on a real DAP.

DAP's flight control software uses an unconventional mixture of spacecraft and aircraft control techniques. Flight simulations confirms that this controls approach enables the platform to consistently reach successive waypoints over the month-long flight simulations.

The ability of DAP to transition between the sailing mode (i.e., cable tension is high) and standard formation flight (i.e., cable tension is low) is a vital capability (e.g., to enable intermittent turns while stationkeeping). A new method to perform these transitions has been identified and characterized with flight simulation which requires special aircraft modifications.

The energy-usage of the DAP configuration during two month-long stationkeeping missions over central Florida (i.e., stationkeeping over Orlando) is evaluated and compared to that of a pure solar aircraft of the same weight and aerodynamic performance. DAP is shown to consistently reduce net propulsion usage while simultaneously increasing solar energy capture.

A baseline 700 GHz communications system is described and its performance evaluated for the proposed mission over central Florida. It is found that the variable roll orientation of the aircraft would increase the power required to maintain coverage over the stationkeeping radius of 150 miles (e.g., by as much as 100% when DAP is 150 miles from Orlando), compared to level flight. This effect can be mitigated via additional antenna design complexity or a more restricted stationkeeping radius.

In summary, the results of realistic month-long flight simulations suggest that the DAP concept may be a viable alternative to the pure solar aircraft as a stratospheric communications relay.

# Table of Contents

# 1.0 Introduction

## *1.1 Background*

Aircraft platforms which could stationkeep in the stratosphere for years, referred to as *atmospheric satellites*, represent a long-standing, grand challenge to the aeronautics community, and have enormous potential societal and economic impact. Such platforms would diversify and expand surveillance capabilities (e.g., NASA's earth science missions) and communications bandwidth and availability (e.g., for underserved remote areas of the US, emergency communications), at a fraction of the cost of orbital satellite networks. Constellations of such platforms might potentially be integrated into the National Airspace System (NAS) to facilitate inter-aircraft communications or to support navigation or for aircraft surveillance. Constellations of such platforms could also improve communications and surveillance capabilities along major shipping lanes.

NASA's Pathfinder and DARPA's Vulture programs, and more recently industry, has funded development of aircraft which rely on solely solar power for propulsion, as shown in Figure 1. These vehicles must accumulate and store a substantial amount of power during the day to operate at night. This is further compounded by the large variability of available solar energy during the year and the inability to point aircraft wings towards the sun to improve solar power capture. These factors result in severe limitations on the power that can be made available to the payload for communications, surveillance, etc.

Figure 1. Stratospheric solar aircraft development efforts (top: AeroVironment's Helios, Boeing's SolarEagle; bottom: Google's Solara, Airbus' Zephyr, Facebook's Aquila)

### *1.2 Dual-Aircraft Platform Concept*

The Dual-Aircraft Platform (DAP), illustrated in Figures 2, is a patented concept for achieving a low-cost atmospheric satellite [1,2] which utilizes wind shear as the primary energy source, and has the potential to stationkeep for years at a time, while providing substantial levels of power for its payload. DAP consists of two glider-like Unmanned Aerial Vehicles (UAVs) connected via a thin, ultra-strong cable which literally sails without propulsion, using levels of wind shear commonly found in lower Stratosphere (e.g., near 60,000-ft). The two aircraft are positioned at different altitudes, as far as 2,000-ft apart, to encounter substantially different wind velocities. The device operates similar in principle to a kite-surfer (see corner image) in which the upper aircraft, referred to as the *SAIL*, provides lift for both aircraft and aerodynamic thrust, while the lower aircraft, known as the *BOARD*, primarily provides an upwind force to keep the platform from drifting downwind (also like the keel on a sailboat).

The aircraft derive power from solar cells, like a conventional solar aircraft, but also extract wind power using the propeller as a turbine when there is an excess of wind shear available. Power is needed to operate the avionics, flight controls, for intermittent use of propulsion, to retract cable, and for the payload.

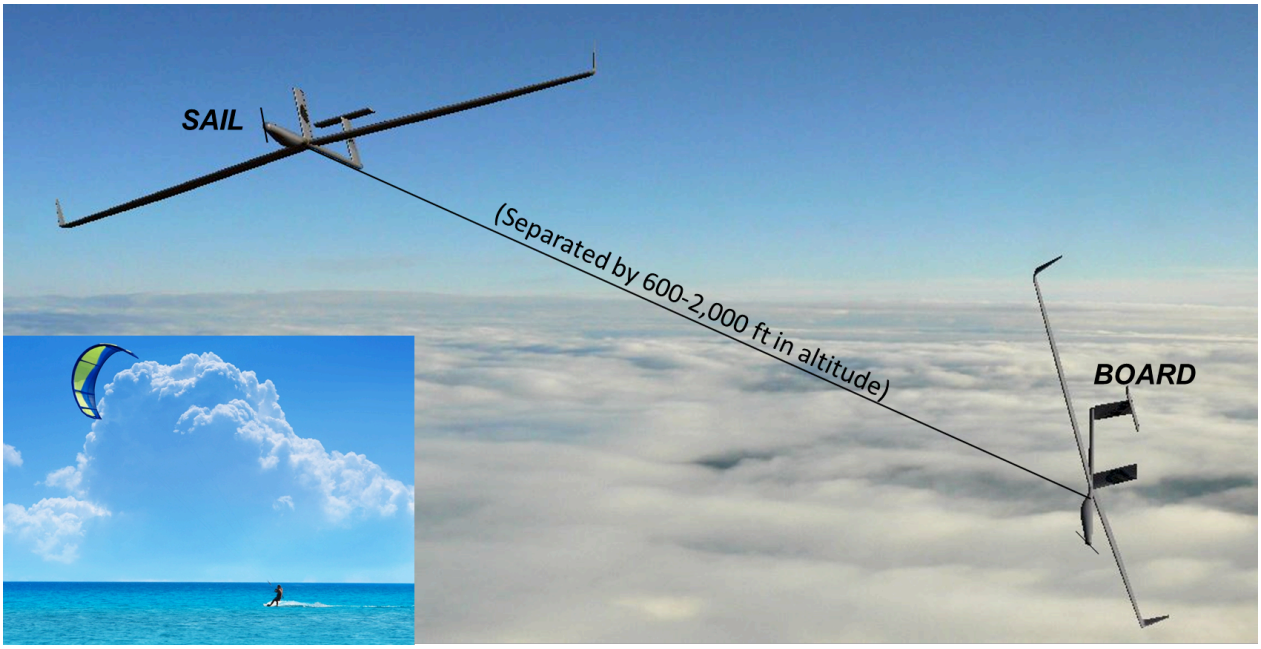

Figure 2. Dual-aircraft platform in sailing formation (aircraft scaled-up in size for clarity)

The theoretical basis of the DAP sailing concept is described in detail in a recent AIAA conference paper [1]. The guidance algorithm uses the atmospheric wind profile to determine the required aircraft altitudes, platform's ground speed and heading, aircraft orientations, cable tension, and lateral (horizontal) spacing using a constrained non-linear optimization problem. Provided stringent but realizable targets for aerodynamic and structural performance are met, it has been shown theoretically that the device could achieve sailing conditions without propulsion roughly 99% of the time within 60,000-70,000 ft.

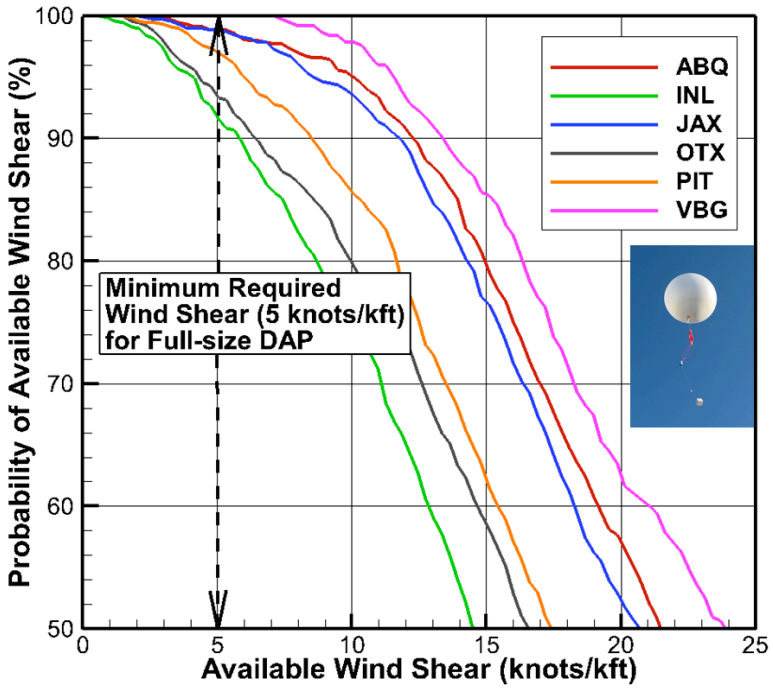


Figure 3. Probability of a wind shear magnitude at 60-70kft for sample of U.S. sites (ABQ: Albuquerque, INL: Inter. Falls, JAX: Jacksonville, OTX: Spokane, PIT: Pittsburg,VBG: Vandenberg)

This theoretical analysis uses wind profiles from the National Weather Service (NWS) radiosonde program, which are measured twice a day at many sites across the country (i.e., about 700 profiles per year per site). A wind shear of 5 knots/1000 feet (or 10 knots across 2000 feet) has been shown to be sufficient for DAP operation [1]. Figure 3 shows that the probability of (at least) a given magnitude of wind shear occurring between 60,000-ft and 70,000-ft, and within a maximum altitude change of 3000 feet, for several radiosonde launch sites. The probability of sufficient wind shear varies between 96%-100% for these sites. However, radiosondes can drift significantly during ascent and provide limited spatial resolution of wind profiles with altitude. Consequently, a major focus of the Phase I effort (to be discussed below) was to develop a more accurate atmospheric model.

### *1.3 Phase I Objectives*

The primary objective of the Phase I effort is to realistically compare the performance of a conventional solar aircraft with the baseline DAP for a specific mission as a communication platform. Two separate month-long flights during which the aircraft must remain within 150-miles of downtown Orlando (see Figure 4) are simulated such that an appropriate line-of-sight is maintained for communications with subscribers in the region. The upper aircraft is to provide power to a payload which enables users below to connect to a cell tower or wi-fi hotspot. The main criterion of evaluation is to compare the daily net energy-usage of the DAP with a pure solar aircraft. The solar energy capture and net energy made available to the onboard payload are also comparison criteria. The following tasks were completed to meet this primary objective:

## Principal Tasks

1. Refine aircraft configuration design to enhance sailing mode of flight performance.
2. Develop realistic atmospheric model using NASA KSC's 50 MHz Doppler Radar.
3. Develop an effective *DAP* guidance strategy to define "waypoints" for the transient atmospheric model.
4. Develop the *DAP* flight control strategy to enable reliable long duration flight simulation
5. Compile performance statistics (i.e., power usage and capture) for both DAP and a pure solar aircraft using flight simulation.
6. Define a communications payload concept for DAP and evaluate its performance relative to solar aircraft carrying the same payload, as well as existing communications systems (vs. Iridium).


Figure 4. Station-keeping boundary of 150-miles around Orlando

## 2.0 DAP Aircraft Configuration

An important product resulting from this effort is a new "twin" DAP aircraft configuration for the SAIL and BOARD, depicted in Figure 5. A twin configuration will reduce development and unit costs as the DAP program moves towards flight demonstrations in the future. The aircraft use a low-Reynolds number, cambered airfoil, and a deformable tailing edge (i.e., flaperons) to offer a relatively large glide-slope (i.e., aerodynamic efficiency) over a large range of angles-of-attack, which is vital for strong sailing performance. The aircraft wings are assumed 80% covered in solar film on both upper and lower surfaces (unlike a conventional solar aircraft which could only benefit from treatment of the upper surface).

The size and mass targets listed on Figure 5 is assumed to be attainable based on comparisons to stratospheric solar aircraft (e.g., similar to Helios @ 0.8 lb/sqft), although no detailed structural design has been conducted. This aircraft structure would need to be heavier and more structurally stiff than a conventional solar aircraft to handle the 3-g wing loads that are found to be typical of the sailing mode. DAP would also not be nearly as vulnerable to wind gusts as a pure solar aircraft. DAP would require a much smaller energy storage system for overnight operations due to use of sailing mode of flight, as will be shown.

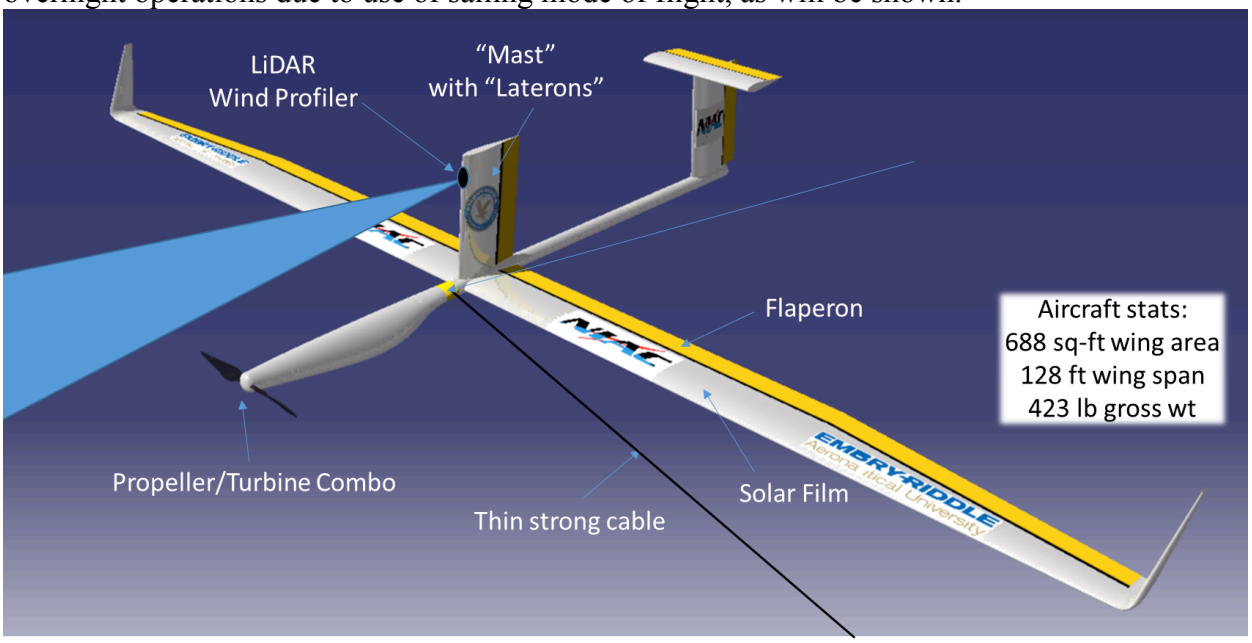


Figure 5. Stratospheric DAP aircraft configuration used for flight simulations

### *2.1 Mast with Laterons*

The fixed "mast" surface atop the main wing with moveable "lateron" control surface is unorthodox but found from flight simulation to enable smoother *transitions* between sailing (i.e., high cable tension) and standard cruise (i.e., low cable tension; near level flight) modes of operation. It is found that this control surface enables faster lateral (y-directed) force response than the conventional method of rolling the aircraft, which has to overcome a relatively large roll

moment of inertia. The potential interference of the wake from this surface with the vertical stabilizer has been neglected in this study.

### *2.2 LiDAR Wind Profiler*

A miniaturized LiDAR wind profiler is also positioned within the "mast" for an unobstructed view to *forecast* the incoming wind shear. Early efforts at long-term flight simulations with small to no forecasting (i.e., no advance knowledge of the incoming wind conditions) led to unacceptable performance. LiDAR is assumed to obtain profiles 3-5 minutes ahead of the current DAP position (i.e., approximately 4 km ahead based on typical airspeed) and roughly 1 km above and below the aircraft altitudes (i.e., assuming a 30° conical region is measured).

Advancement in LiDAR wind profiling technology at NASA includes successful demonstration of onboard LiDAR wind profilers. For example, NASA GSFC's TWiLiTE program demonstrated use of an onboard Doppler wind profiler using the NASA ER-2 high altitude aircraft [3], as well as on Global Hawk. NASA Langley's Doppler Aerosol Wind (DAWN) program [4] has demonstrated high-accuracy LiDAR-based wind profiling on the DC-8 aircraft. However, the weight and power usage of these systems are too large for use on DAP.

NASA Langley's Laser Remote Sensing Branch has demonstrated that LiDAR systems for navigation can be significantly miniaturized [5]. Figure 6 below shows a NASA Langley's 2012 prototype miniaturized LiDAR system chassis for navigation, weighing less than 16.4 kg and requiring only 95 W of power and having range of 2.5 km. A much lighter (10 kg), more energy efficient (85 W), and longer range (4 km) LiDAR chassis is to be completed in 2016 (shown to the right). In correspondence with Dr. Farzin Amzajerdian from NASA Langley's Laser Remote Sensing Branch, he suggested that a miniaturized LiDAR wind profiler system that meets the specifications required by DAP (i.e., for weight, power, range) could be developed within two years.


Figure 6. Miniaturized LiDAR chassis developed at NASA Langley in 2012 and 2016

### *2.3 Cable Connection System*

The cable connection system is configured to accommodate retraction/extension of the cable, and avoid cable-to-aircraft impingement. The cable material is currently chosen as

Dyneema, an ultra-high-molecular-weight polyethylene fiber, as depicted in Figure 7. An off-the-shelf 3.0-mm diameter braided cable like that shown in Figure 7 (left) provides a breaking strength of 2700 lbf, according to the vendor, which is several factors more than the platform can create during cruise at maximum lift. A strong dynamic component (i.e., the aircraft must move apart at speed of roughly 20 knots, relative to each other, to break the cable.

The *SAIL* aircraft trajectory is constrained to fly ahead of the BOARD such that there is no cable-to-aircraft impingement of the *BOARD*. The center of gravity (cg) of the aircraft is located just in front of the main wing to permit connection of the cable directly to the cg (see gold cylinder), which minimizes aircraft-to-aircraft induced moments. The forward position of the CG results in an acceptable loss of aerodynamic efficiency due to the need for a larger horizontal stabilizer and/or tail boom. The gold cylinder on the *SAIL* aircraft includes an electrically-powered "fishing-reel" (winch) mechanism to adjust cable length in-flight. The gold cylinder on the *BOARD* contains a "roller-bearing" mechanism to permit free aircraft rotation while connected to the *SAIL*, as depicted in Figure 7 (right).

Figure 7. Elements from Cable Connection System. Dyneema Cable (left); Tapered Roller Bearing on *BOARD* (outer section rotates freely)

### *2.4 Propulsion/Turbine System*

The electric propulsion system is configured to include 1.5 meter long blades electric propeller blades (i.e., 3 meter diameter) which are extendible/retractable to minimize drag during cruise. These blades and are also assumed to unconventionally be used to extract wind power in a "turbine mode" via variable pitch and twist. A propeller-driven sport aircraft that can extract energy during descent has been developed and demonstrated by Pipestral (Figure 8). The maximum power and weight of this propulsion/turbine unit of 85 kW and 14 kg are close to the level of power and weight required by the DAP. It is speculated that a similar device could be developed for use in the lower stratosphere.

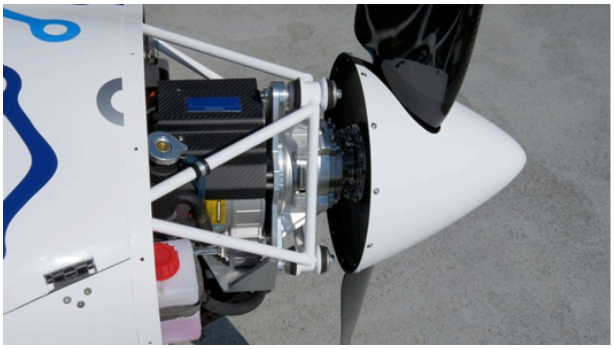



Figure 8. Pipestral's WattsUP Prototype with propeller that can extract wind energy as a turbine

### *2.5 Aerodynamics Assessment*

An important aspect of developing a new aircraft configuration is to produce credible aerodynamics performance data for use in the flight simulations. XFOIL is used to evaluate 2-D airfoil performance, which is adjusted for 3-D finite-wing effects (e.g., adding induced drag). The effects of control surfaces and the dynamic stability are introduced using linearized aerodynamics coefficients obtained from a vortex lattice method (VLM) solver, *Tornado,* distributed under a GNU-general Public License. The profile and skin friction drag for the fuselage is estimated based on typical glider values. The maximum lift-to-drag of the baseline configuration is approximately 35 at a typical sailing flight Reynolds number of 500,000. For purpose of simulation, appropriate limits are imposed on control surface deflection, deflection rates, as well on the thrust response.

A more detailed aerodynamic characterization is unwarranted at this early stage in development. However, it should be emphasized that the guidance software requires accurate characterization of the aircraft aerodynamics to enable providing sailing mode flight conditions. Consequently, the aircraft aerodynamics will eventually need to be characterized using a combination of high-fidelity numerical analysis and extensive flight testing.

## 3.0 Atmospheric Model derived from KSC Doppler Radar Wind Profiler

A crucial element of the study was to develop a high fidelity transient atmospheric model possible for long-duration flight simulations near 60,000 feet (18.3 km). Empirical databases exist to estimate wind profiles for a given time of the year, like the Earth Global Reference Atmospheric Model offered by NASA Marshall Space Flight Center. These databases offer accurate statistical representations of the winds at a given altitude and time of year. However, we opted instead to build a unique, high-fidelity model based on high-temporal frequency atmospheric profiles measured by the 50-MHz Doppler Radar Wind Profiler (DRWP) over KSC. Mr. Ryan Decker, from the MSFC Natural Environments Branch (NEB), utilized archived DRWP-measured wind profiles over KSC and weather balloon observations to produce two separate long duration (i.e., 30 and 39 day) transient atmospheric environments which the DAP would encounter at flight altitudes between 15-18.5 km. Winter season cases were selected for DAP performance assessments as the winter season in central Florida exhibits the most variability/dynamic environment annually. These cases were representative of the upper atmospheric climatology over central Florida.

i. ***February 10$^{th}$ to March 11$^{th}$ (2011) – 30 days***
ii. ***January 17$^{th}$ to February 24$^{th}$ (2006) – 39 days***

An additional case was provided consisting of continuous sample of DRWP measurements with high frequency gust added to the profiles to assess gust effects in the DAP simulations. A brief summary of the meteorological data sources, selection criteria, analysis and inclusion of simulated high-frequency wind gust will be described below.

### *3.1 Data Sources*

A key element of the task is to use measured wind and thermodynamic data as opposed to statistically modeled data. In meeting this element, the task is making use of a wind database, developed by the NEB, of high temporal resolution tropospheric wind profiles at Kennedy Space Center from measurements by a 50-MHz Doppler Radar Wind Profiler (DRWP) along with thermodynamic profiles from rawinsonde measurements [6] over the period 1997-2012. The DRWP operates nearly continuously and is used to support launch operations at KSC and the United States Air Force's Eastern Range at Cape Canaveral Air Force Station (CCAFS). Wind profiles are generated every 3-5 minutes at 150-m intervals from 2-18.5 km. Because DRWP radar signal return is sensitive to anomalous signal returns due to hydrometeors, sidelobes, etc. the NEB developed extensive data quality checks to apply to the data in an effort to remove erroneous data and/or entire profiles [7]. The resultant database was used to select profiles for this task. The thermodynamic data was obtained from rawinsonde Measurements at CCAFS. Rawinsonde profiles contain wind, pressure, temperature, relative humidity and density data reported at ~350 m (1000 ft) intervals. The resulting uneven reporting intervals between the DRWP and rawinsonde data had to be rectified. Since the vehicle performance is more sensitive to winds, the thermodynamic data were interpolated to 150-m altitude intervals for consistency with the DRWP data. Profiles provided for DAP flight simulations consisted of wind speed and direction, pressure, temperature and density at 150 m intervals for 23 discrete altitudes from 15-18.5 km.

### *3.2 Selection Criteria*

A series of criteria were used to find valid cases for use in the DAP simulations. Climatologically, the winter season in central Florida is the most dynamic wind environment so cases for this study were chosen from winter months between December and March [8]. The goal was to find a case consisting of 60 consecutive days. This was an aggressive goal as primary application of the DRWP database was for space launch vehicle performance assessments and climatological applications where having continuous data were not essential. Therefore, there are numerous periods of missing data, sometimes entire days, throughout the database making it difficult to find long periods of continuous data. The first examination of the database consisted of determining if profiles for each day existed and the database was constructed with data partitioned into daily files containing all the profiles for that day. When a day did not have any profiles a file would not exist. For each winter season over the 15 year period of record, the largest number of consecutive days was determined by counting the number of continuous days where profiles exist. Cases where consecutive days were greater than 30 were kept for further evaluation. The next step was to determine the number of consecutive missing profiles that existed over the time period of those selected cases. It was known there would be missing profiles so in order to limit the number of case rejections because of missing profiles a criteria was used that would keep cases if less than a certain number of hours of consecutive missing data existed. This criterion is based on the time interval that vertical wavelengths would no longer be correlated [9]. The vertical wavelength filter defines the boundary wavelength, as a function of time, between correlated and non-correlated wavelengths within the wind profile. Cases where more than 9 hours, corresponding to wind feature wavelengths of ~3.2 km, existed between missing profiles were rejected. This method was used to preserve the correlation between the profiles that exist on either side of a missing data gap by preserving the persistent characteristic of the wind through wavelength filtering the wind profile on either side of the data gap and then performing linear interpolation across the profile gap to replicate those missing wind profiles. A 9-hour time gap is a valid approximation, as winds in the upper troposphere vary on longer time scales than winds near the surface. There were two cases that did not have missing profiles gaps that exceeded 9-hours over a period longer than 30 days; January 17 to February 24, 2006 and February 10 to March 11, 2011.

Throughout the period in both cases missing profiles existed. Several methods of filling in the missing wind data were used. When a single profile was missing, the wind profile would consist of linearly interpolating the data from the profile before to the profile after the missing time. If there were more than one missing profile between valid profiles then the missing profiles would be generated through a technique of filtering the entire wind profile that occurred on either side of the missing data period followed by linearly interpolating the data at evenly spaced time intervals over the missing profile time period. The wavelength filter is based on the length of time between the two measurements as described in the previous section. This approach keeps the synthetic profiles correlated to the measured profiles at the longer wavelengths and for smooth transition over the period of missing data. There were 11 periods of synthetic wind profiles ranging from 0.33 to 8.5-hrs in the 2006 case and 6 periods ranging from 0.25 to 4.0-hrs in the 2011 case. The thermodynamic data for these two periods were included from weather balloon measurements at the CCAFS. The atmospheric temperature, density and pressure data

were added to the DRWP wind profiles. The thermodynamic measurements are typically made every 12 hrs. For the DAP simulations, it was adequate to linearly interpolate the thermodynamic data to the time interval of the wind profiles. This was performed on the thermodynamic profiles in the 2011 case. However, for the 2006 case the majority of the days did not have weather balloon measurements so a climatological sample of thermodynamic data from the 2013 CCAFS Range Reference Atmosphere (RRA) database was included in the wind profiles. The RRA database profiles monthly climatologies of wind and thermodynamic statistics (mean, standard deviation, etc.) from weather balloon measurements over an ~20 year period [8].

### *3.3 Data Analysis*

Since there were only two cases provided and comprised of only a small sample of the upper atmospheric environment, statistics from these cases were compared against an independent database to determine how the cases compared against climatology. The mean of all the variables for each case were calculated and plotted against the mean, "mean + 3-sigma" and "mean – 3-sigma" February climatology from the CCAFS RRA. The data was plotted against the month of February only since it contained the majority number of profiles for both cases. Wind speed and direction data were converted to U and V components. The mean wind components for both cases closely resembled the RRA monthly mean as shown in Figures 9-10. Likewise the thermodynamic data closely followed the RRA monthly mean for the 2011 case. The 2006 case was not compared since the thermodynamic data in the profiles used the RRA data. These results verify these cases are valid representations of the upper atmospheric environment over central Florida.

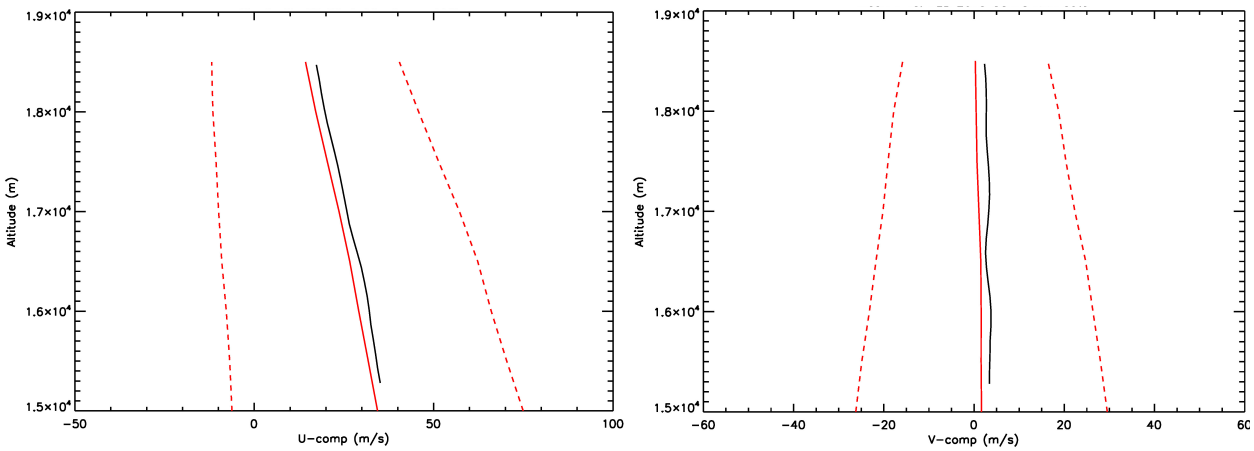


Figure 9. Mean U- (left) and V-components (right) from 2006 case represented by the black solid line. Red solid line is the representative mean wind component from 2013 CCAFS RRA. Red dashed lines are the "mean – 3-sigma" and "mean + 3-sigma" curves.

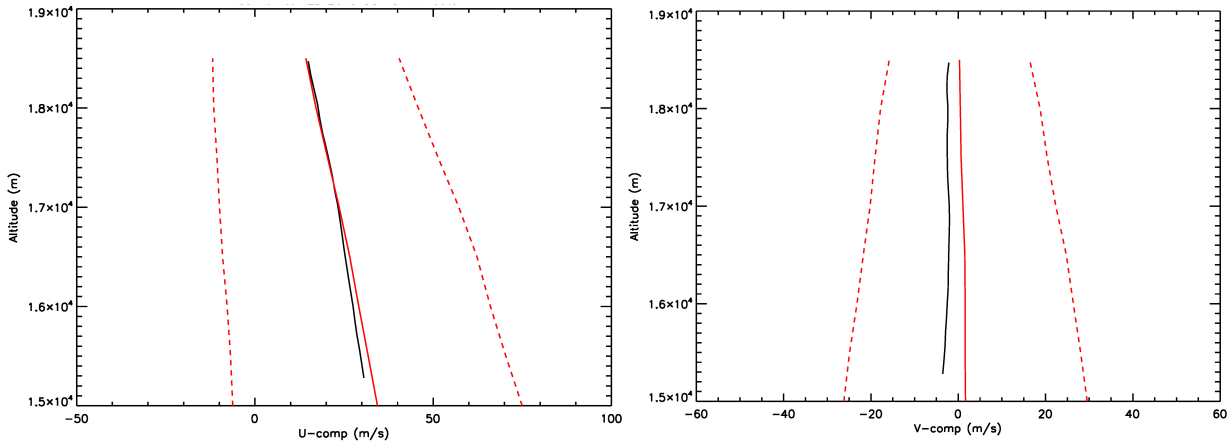


Figure 10. Mean U- (left) and V-components (right) from 2011 case represented by the black solid line. Red solid line is the representative mean wind component from 2013 CCAFS RRA. Red dashed lines are the "mean – 3-sigma" and "mean + 3-sigma" curves.

### *3.4 Gust Content*

In the actual flight environment, the DAP will be exposed to wind profiles with wavelengths that are smaller than those measured by the DRWP. An additional case was provided that enhances the wind profiles by simulating wind gusts at wavelengths smaller than those resolved by the DRWP. The simulation process used an approach based on the power spectrum density (PSD) of wind components and extrapolating the total perturbation energy down to the wavelength of interest. The case provided had continuous DRWP measurements over a 6-day period and were enhanced with wind gust content down to 30-m wavelengths.

The typical range of wind speed profile variations due to this gust energy are projected to be less than ±2 m/s from this initial examination. Although a modest gust effect, a detailed treatment of gust effects using the Dryden Wind Turbulence Model within previously described the Simulink/Matlab flight environment should be included in future efforts.

### *3.5 Atmospheric Model Examination*

A cursory examination of the atmospheric datasets show that sufficient levels of wind shear to enable the DAP sailing mode of operation are persistently available. Figure 11 (top) shows a hypothetical altitude history over the first 24-hour period of the aforementioned 39 day data set. Despite trajectory restrictions of a constant 2,000 ft altitude separation between the SAIL and BOARD aircraft, and a limit on ascent/descent rates of 2 ft/sec, the platform would be able to "find" more than sufficient wind shear (i.e., > 10 knots wind differential) to permit sailing for the entire 24-hour period as shown in Figure 11 (bottom). Over the 39 day dataset, the platform remains above this 10 knot differential for 93% of the duration. This assumes that the aircraft can "forecast" the wind profiles 3-5 minutes ahead using an onboard LiDAR wind profiler. Note that if sufficient wind shear is present, propulsion is not necessarily needed to ascend, and wind energy may be extracted by using the propeller as a wind turbine, reducing the net energy required to remain aloft. Although the DAP trajectory determination is not this simple, this examination strongly suggests that persistent wind shear is available to support the sailing mode of operation.

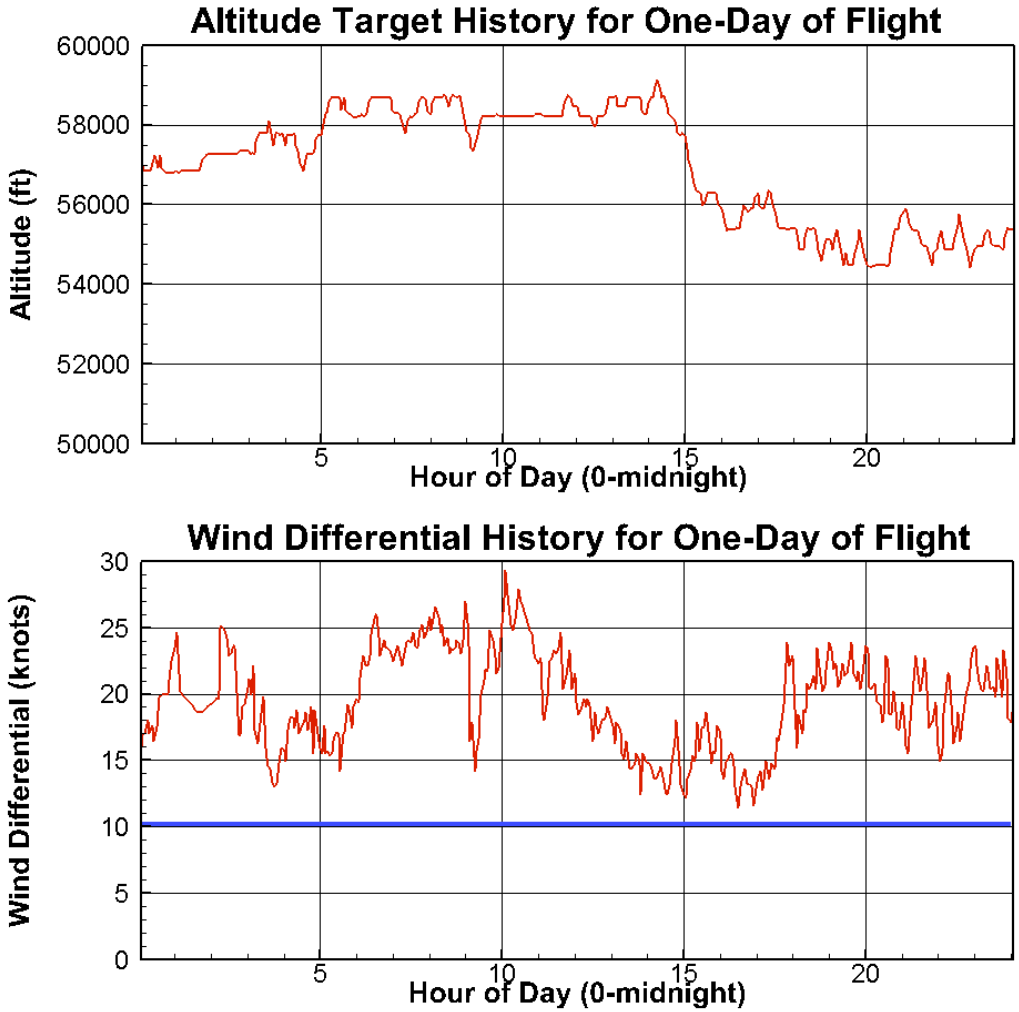


Figure 11. SAIL altitude history and corresponding wind differential across platform during one 24-hour period

To our knowledge, this dataset represents the highest fidelity environment available for simulation of flight at this altitude range of 50-60 kft. This dataset is an important product because it is applicable to the emerging genre of atmospheric satellites.

# 4.0 DAP Flight Software Development

DAP flight software has been developed to enable robust long duration flight simulations using the aforementioned DAP configuration from Section 2.0 and high-fidelity transient atmospheric models from Section 3.0. This software environment consists of three main software components of guidance, flight control, and flight simulation, which are described below. The first sections deal with the original FORTRAN software environment that has been refined in this study, and the last sections deal with a new SIMULINK-MATLAB hardware-in-the-loop flight simulator that has been developed during this study.

### *4.1 DAP Guidance Software (Sailing Flight Operations)*

DAP's guidance software is written in FORTRAN90 by Dr. Engblom at ERAU and uses a constrained nonlinear optimization technique to determine the optimal aircraft altitudes, speed, heading, orientation, and lateral spacing for sailing mode in a given atmospheric profile [1]. Specifically, the sailing mode involves cruise at constant platform speed and heading – a "pseudo-steady soaring" mode of flight as opposed to the well-known dynamic soaring approach. Unlike conventional waypoints that consist of target positions versus time (i.e., a simple trajectory), the DAP waypoints represent a more complex state of ten (10) variables necessary to achieve sailing mode of flight, including:

- $Z_S$ (*SAIL* altitude)
- $Z_B$ (*BOARD* altitude)
- $V, \gamma$ (platform ground speed and heading from North)
- $\alpha_S$, $\phi_S$ *(SAIL* angle-of-attack and roll angles)
- $\alpha_B$, $\phi_B$ *(BOARD* angle-of-attack and roll angles)
- $X_{SB}$ (*SAIL* distance from BOARD in *X*, North)
- $Y_{SB}$ (*SAIL* distance from BOARD in *Y*, East)

The sideslip angle is zero as a consequence of the Euler angle rotation sequence of yaw-roll-pitch, where the yaw rotation puts the aircraft directly into the relative horizontal wind. If sailing is not possible, a more conventional yaw-pitch-roll sequence is used with an additional explicit constraint on the sideslip angle.

This software is now modified to calculate these flight conditions (or "waypoints") every 3-5 minutes to correspond with the time-varying atmospheric model profiles developed by NASA-MSFC. A series of constraints are imposed in the optimization technique to produce smooth variation in these waypoints to improve flight controllability and minimize energy usage. Additional constraints are needed to promote aircraft safety, including, but not limited to:

- Altitude range limits (50,000 – 62,000 feet)
- Maximum allowable dynamic pressure (structural limit)
- Maximum allowable cable tension (limited by tensile strength and safety factor)
- Maximum extended tether length (limited by cable length)
- Minimum allowable angle of cable relative to SAIL yaw plane (avoid cable contact)

- Range of allowable angle of cable relative to BOARD roll plane (avoid cable contact)
- Minimum allowable tether tension (must always be positive to be in tension)
- Range of allowable angle-of-attack

This software currently identifies target platform state conditions that permit sailing mode of flight (i.e., without propulsion) for greater than 90% of the duration of both of the 30+ day atmospheric models. When the sailing mode of operation is not available, the guidance software establishes a waypoint for which the use of thrust is minimized.

Occasionally the software requires significant computational effort to complete the optimization process. It is concluded that waypoint solutions may need to be generated and tabulated for a wide range of potential atmospheric conditions and stored onboard for quick retrieval.

### *4.2 DAP Guidance Software (Transition Flight Operations)*

The guidance software will require DAP to make "transitions" between the sailing flight mode and a formation flight mode. For example, DAP must intermittently complete near 180° turns to fly back towards the center of the service area (i.e., to stationkeep). Before a turn the platform must transition from sailing mode to formation flight mode, and after the turn, the platform must transition back to sailing mode. Also, when the platform must make a considerable change in altitude (or even in lateral spacing), the platform will need to transition into formation flight before making these changes in the flight conditions, and then transition back to sailing mode when appropriate.

These transitions are not trivial. First, the cable tension is relatively large during sailing flight mode and nearly slack during formation flight. The *BOARD* aircraft often operates at roll angles of approximately 90° while sailing, but must regain level flight when in formation. Additionally, there is potential risk for cable-to-aircraft impingement during these transitions if not sufficiently controlled. These drastic changes represent a significant controls challenge. Consequently, a smooth and low-risk style of transition is desirable.

The FORTRAN90 guidance software currently creates a series of "mini-waypoints" to support these transition maneuvers which takes a few seconds of real time to compute. These waypoints represent pseudo-steady flight conditions that enable a smooth and safe transition. The key element for success, discovered during this Phase I effort, is to connect the cable to the *BOARD* aircraft just ahead of the main wing and permit free rotation via a "roller-bearing" mechanism. Flight simulations show this style of transition to be relatively safe. The additional use of the mast and lateron control surface permits faster and safer transitions, but successful transition without the mast surface have been demonstrated in flight simulations.

Figure 12 provides a snapshot of before and after a "transition" simulation from a standard flight formation mode (top) to the sailing flight mode (bottom). Note that the tension in the cable (at the *SAIL* attach point) is relatively weak (~70 N and slackness is evident) while the aircraft move in formation in effectively steady, level horizontal flight. The aircraft are pointed into their respective relative winds. The *SAIL* appears larger since it is at a higher altitude, and the aircraft images are only placeholders for the actual shape. The tension and tightness in the cable grows steadily as the aircraft reach the sailing flight condition, to maximum levels of nearly 600 N in this case. It is important to note that such a transition has not been done in real world flight to our knowledge, but this physics-based simulation suggests that it can be done

without the aircraft losing control or impinging the cable. This transition is defined by a series of "mini-waypoints" spanning about forty-seconds of real-time, using an optimization procedure which typically takes a few seconds of real-time to compute, and utilizes a waypoint condition provided from the aforementioned, main guidance software.

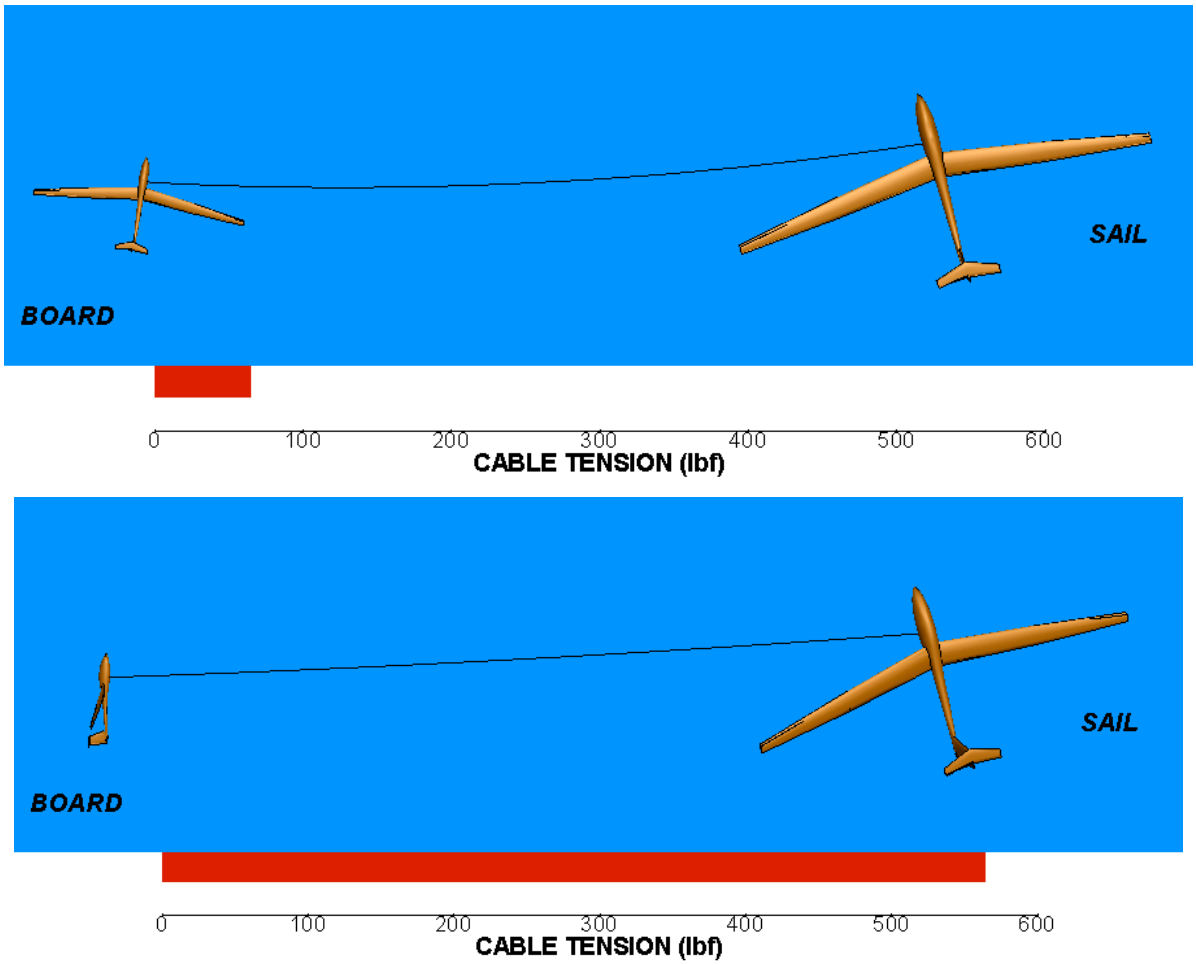


Figure 12. Start and end images of animation of the transition maneuver from "standard" to "sailing" flight modes

### *4.3 DAP Flight Controls Software*

The flight controls logic uses a combination of quaternion-error based attitude control, traditionally used by from spacecraft to reach target Euler angles. The flight controls logic also uses thrust, lateron, and flaps for the X-, Y-, and Z- body frame velocity and position control, respectively. PID controllers have been tuned for this six degree-of-freedom controls approach, and have enabled successful completion of flight simulation using the long duration (i.e., 30 and 39 day) atmospheric data sets. Note that, conventional aircraft use roll adjustments to alter lateral speed and position, but this approach was not investigated or utilized in this study to avoid increasing potential of cable-to-aircraft impingement. The controls logic also contains special provisions for when the aircraft must make a significant climb or descent. It should be pointed

out that a more sophisticated adaptive controls technique to replace the PID controllers would be worth investigation.

### *4.4 DAP Flight Simulator*

DAP's flight simulator is based on open source code originally developed at NASA Langley and available in FlightGear to handle the 6-DOF dynamics and control of a rigid aircraft. The open source portion, originally written in C, has been converted to FORTRAN90. A multi-degree-of-freedom segmented cable model is integrated into the code to handle the cable dynamics and interactions between the two aircraft. The cable is typically simulated as twenty equal length segments. Wave speed propagation of disturbance initiated at one end of the cable, between aircraft, depends on the tension level, and has been verified from flight simulation to approximate theoretical wave speed values for the selected cable material of Dyneema.(i.e., typical wave speeds of 500 m/s to 1 km/s). These high wave speeds are essential for the aircraft to "communicate" and operate efficiently.

The aerodynamic forces on the cable are a major limitation of sailing performance. These forces are modeled based on Hoerner's method for a cylinder in crossflow. Based on the low Reynolds numbers involved, a normal force coefficient of 1.0 is imposed across the cable, and a skin friction coefficient of 0.02 is imposed along the cable.

### *4.5 New Simulink-based DAP Flight Simulation Enviroment*

A new ERAU Flight Simulation Environment was developed to support future design and testing of algorithms for DAP flight capabilities (e.g., in a Phase II). Although the FORTRAN-based flight simulation capability has been used for all flight simulation results presented in this report, this new Matlab/Simulink environment will provide greater flexibility and capability relative to development of the flight software to be used onboard a future flight demonstrator.

A modular structure within Matlab/Simulink interfaced with FlightGear and X-plane for visualization was adopted for maximum portability, flexibility, and extension capability. The simulation scenario can be setup to include the following features: manual or autonomous flight, DAP aero model, high fidelity sensor model, formation based flight control system, atmospheric model, actuator and cable dynamics that connect board and sail systems. A modular architecture has been adopted to allow easy upgrade or addition of individual components within a Matlab/Simulink environment, as illustrated in Figure 13.

DAP aircraft equations of motion and multi-degree-of-freedom cable dynamics, combined with lookup tables for aerodynamic characteristics, are solved using Matlab/Simulink functions. Simulation can be run in real time or accelerated time. Comprehensive input/output interfaces include FlightGear and X-Plane (Figure 14), plots, and Simulink scopes.

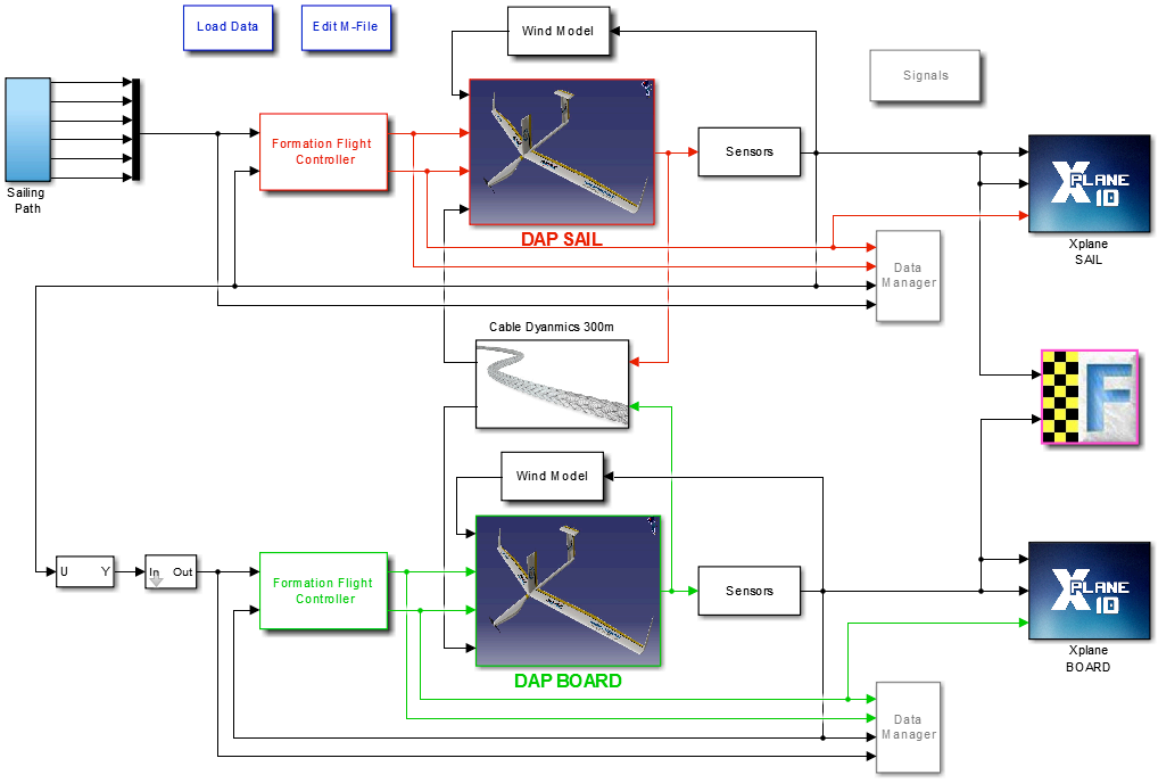


Figure 13. Simulink/Matlab Simulation Environment


Figure 14. ERAU Simulation Environment – X-Plane Interface

### *4.6 DAP Autonomous Flight Control Software for Formation Flight*

DAP flight control logic for autonomous flight in formation (i.e., not for the sailing mode) has been implemented, integrated, and tested within the Matlab/Simulink simulation environment. A conventional fixed-parameter linear control approach is taken in which the general architecture of the control laws is based on an inner/outer loop control scheme. As shown in Figure 15, this configuration is based on a minimization of forward, lateral and vertical distances with respect to a desired trajectory, while maintaining stability and adequate performance.

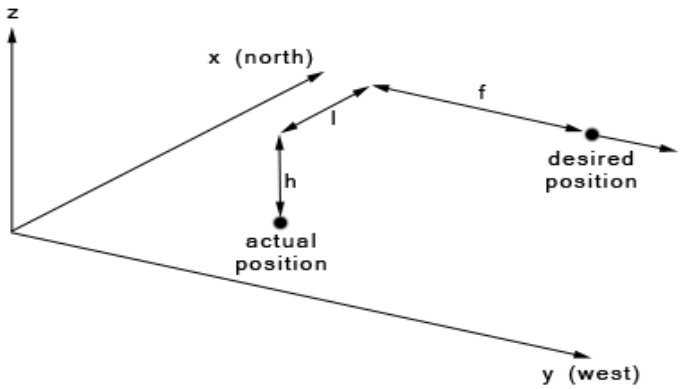


Figure 15. Geometry of Trajectory Tracking Error

The position PID control laws consist of three distinct modules as shown in Figure 16. The first module calculates the forward, lateral, and vertical distance errors and relative velocities from the reference trajectory. Then, an outer-loop module produces the bank angle, throttle, and pitch angle commands that are necessary to compensate for lateral, forward, and vertical errors, respectively, using Equation (1) through (3).

$$\phi_d = K_{\dot{l}}\dot{l} + K_l l \tag{1}$$

$$\delta_T = K_{\dot{f}}\dot{f} + K_f f \tag{2}$$

$$\theta_d = K_{\dot{h}}\dot{h} + K_h h \tag{3}$$

Inner-loop linear control laws use the desired bank angle and pitch angle to produce aileron, rudder, and elevator commands according to Equations (4) through (6).

$$\delta_a = K_p p + K_\phi(\phi - \phi_d) \tag{4}$$

$$\delta_r = K_r r + K_{\phi r}(\phi - \phi_d) \tag{5}$$

$$\delta_e = K_q q + K_\theta(\theta - \theta_d) \tag{6}$$

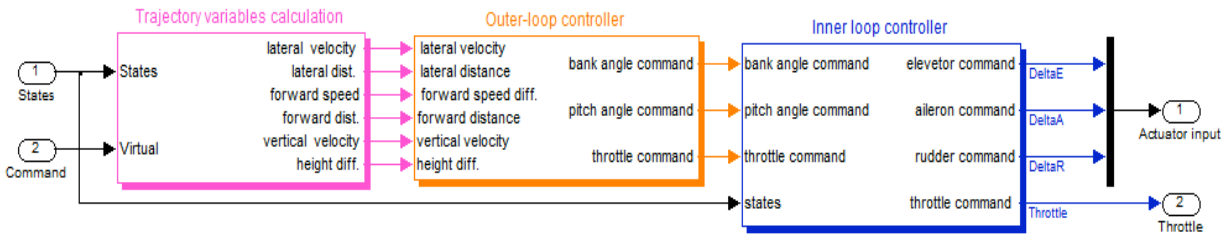


Figure 16. Formation Flight Control System

This DAP autopilot capability has been verified to perform adequately in the flight simulation environment in a simplified, steady atmospheric model without maneuvers (e.g. turns). In the future, the research team could expand the capability of the control system to address all phases of flight. The sailing flight mode and related transition maneuvers could be addressed starting from the logic demonstrated with the previously described FORTRAN-based environment. Also, the team could investigate the implementation of non-linear and adaptive approaches such as non-linear dynamic inversion augmented with L1 and model reference adaptive control laws [10-13] in a future study. It should be noted that this new DAP Flight Simulation Environment can be easily expanded to include additional components and options in all modules (e.g., sensor models, gust treatment).

# 5.0 DAP versus SOLAR Energy Usage and Capture

The results from the two long duration flight simulations of 30 and 39 days are summarized here. The 30 day flight simulation was used to focus on developing a guidance and flight control strategy that results in low propulsive energy usage by the DAP relative to a pure solar aircraft flying solo. The 39 day flight simulation was used to include consideration of solar energy capture during the flight simulations. Consequently, the net energy remaining for onboard payloads is also evaluated with the 39 day flight simulation results.

## *5.1 Methodology behind Energy Usage Estimates*

Daily energy usage by the propulsion system for the SAIL and BOARD aircraft during long duration flight over central Florida are derived from the time-accurate flight simulation results. As previously mentioned, the guidance algorithm defines waypoints every 3-5 minutes which maintain the sailing flight mode and typically do not require "drastic" changes to the platforms flight conditions. When sailing conditions are not possible, a minimal level of thrust is imposed by the waypoint conditions. The flight time intervals associated with the aforementioned waypoints account for typically more than 96% of a given day. The energy usage during these time intervals is simply integrated based on the thrust used (or created in turbine mode) for each second in the flight simulation.

The remaining 4% of the flight duration involves "drastic" changes to the flight conditions (e.g., large altitude change of greater than 1000 ft over the next 3 minutes). For these time intervals, the platform is assumed to transition to a standard formation flight mode to make the necessary changes to the flight condition (e.g., make the altitude change), and then transition back into the sailing mode. Another example which requires these two transitions is when the platform is required to intermittently turn to remain within 150-miles of the starting point of day #1 (i.e., downtown Orlando). These time intervals are not simulated, but rather the energy usage is estimated based on the power required to climb/descend, the duration, and using an assumed formation flight glide slope of 20.

The DAP propulsion system is to provide thrust as needed, and create thrust using the same propeller in turbine mode when there is excess wind energy to extract. Note that the propeller blades may be retracted while another pair of turbine blades are extended, from the same shaft. Or, the propeller blades may have variable pitch and twist capability to offer the turbine mode. The propulsive power and turbine power estimates are based on simple actuator theory (aka momentum theory) based on the required thrust and drag imposed, respectively. A three (3) meter diameter propeller/turbine is specified. Modest propulsive and kinetic energy efficiencies for the two modes are assumed:

- Propulsive Efficiency = 75%
- Turbine Kinetic Energy Efficiency = 25%:

Typical large-scale propeller efficiencies can reach above 85% while typical large-scale wind turbine kinetic energy efficiencies can reach above 40%. However, for the lower Reynolds number application of a stratospheric propeller/turbine, it is assumed these efficiencies would be

significantly lower. A more detailed prediction of the propeller/turbine efficiencies is deemed unnecessary at this early stage of DAP development.

The power required to operate the onboard LiDAR wind profiler, and the power needed to retract the cable during flight, are included to provide a more fair comparison with a pure solar aircraft. Based on correspondence with NASA Langley's Laser Remote Sensing Branch, a 100-W power continuous power usage for a miniaturized LiDAR is a reasonable goal. Assuming a maximum cable retraction rate of 10 cm/s at a typical cable tension during sailing of 3000 N, and a mechanical efficiency of 80%, the maximum power required to retract the cable is approximately 360 W. However, cable retraction typically occurs at less than 2 cm/s in the flight simulations, resulting in less than 72 W. Cable extension occurs at similar rates in the flight simulations but the energy cost is neglected as small. This power may be supplied by an onboard electric winch, or possibly driven off the propulsion system's electric motor. The overall energy impact of the LiDAR and cable winch is deemed minor compared to the propulsive requirements.

The pure solar aircraft used for the evaluations herein, SOLAR, is assumed to have the same size, weight, and aerodynamic efficiency as the DAP aircraft for simplicity. It is presumed that the SOLAR aircraft will have a lower structural weight, but will carry more battery weight compared to the DAP aircraft. For the purposes of comparison, SOLAR is assumed to maintain a near maximum high glide slope of 35 at 60,000 feet, for the entire flight duration, and no account for energy usage for intermittent turns or altitude adjustments has been attempted. SOLAR is assumed to fly at a much lower true airspeed than DAP typically flies, which results in the lowest possible power usage. Consequently, the daily net energy usage for SOLAR is a constant.

### *5.2 DAP Propulsive Energy Usage for 30-Day Flight*

Figure 17 shows the daily energy usage by the propulsion system for the SAIL, BOARD, and SOLAR aircraft for the 30 day atmospheric model described in Section 3. *Twelve days involve negative net energy usage, and all of the days require less than one-third the energy required by an identical aircraft (i.e., size, weight, etc.) flying solo as a conventional SOLAR aircraft.* Excess wind energy is often available, and the propulsion system must create negative thrust (i.e., drag) by operating as a wind turbine, appropriately limited by the available wind (i.e., true airspeed) to maintain steady sailing conditions.

Figure 18 shows the daily energy usage for the same 30 day flight if the wind turbine mode is not permitted. That is, the aircraft would need to create drag using spoilers or other means. Interestingly, the daily energy becomes more consistent from day-to-day and the maximum daily usage is unaffected. Still, DAP requires less than half the energy required by SOLAR.

Figures 17 and 18 are the result of several iterations on the guidance logic to find the approach which leads to minimal daily net energy usage. It should be emphasized that the guidance software makes no attempt to improve solar energy capture. Consequently, there are several days during which one or both of the DAP aircraft capture much less solar energy than the SOLAR aircraft. Nevertheless, these results suggest that propulsive energy requirements can potentially be significantly reduced using the sailing mode of operation.

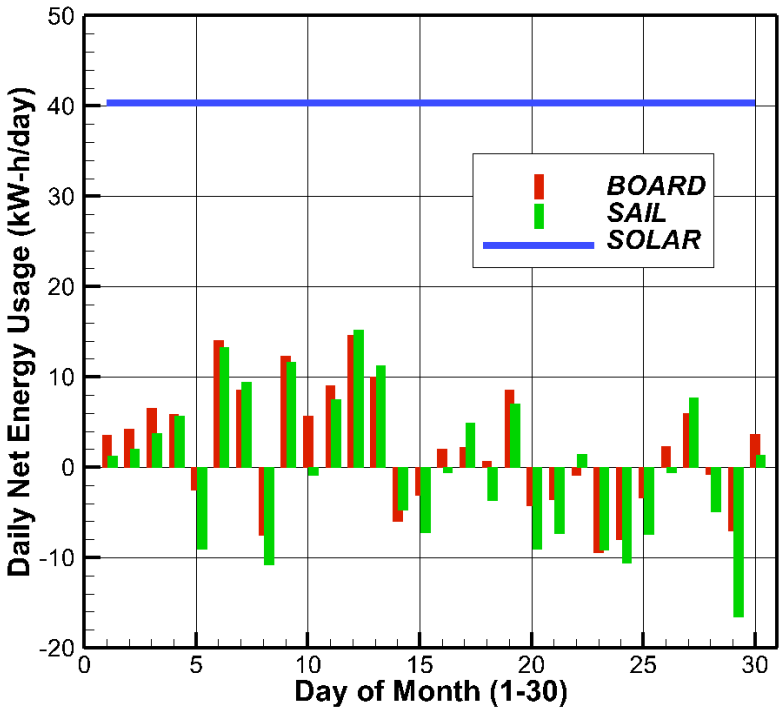


Figure 17. Daily energy usage by DAP aircraft compared to pure solar aircraft over 30 days (turbine mode active)

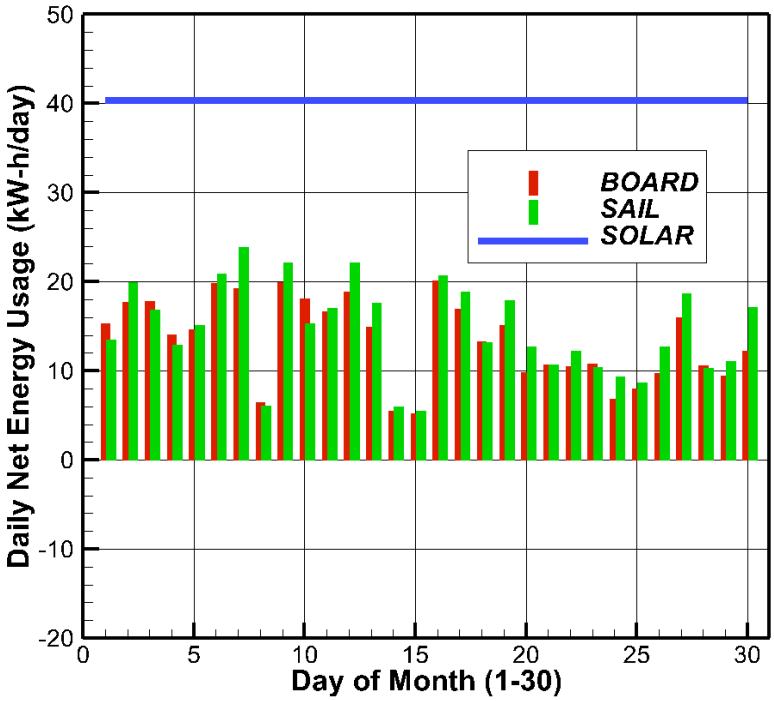


Figure 18. Daily energy usage by DAP aircraft compared to pure solar aircraft over 30 days (turbine mode not active)

### *5.3 DAP Propulsive Energy Usage and Solar Energy Capture for 39-Day Flight*

Figures 19 (left) shows the daily energy usage by the propulsion system for the SAIL, BOARD, and SOLAR aircraft for the 39 day atmospheric model described in Section 3 when the turbine mode is active. In this simulation, the DAP aircraft operate in standard formation flight mode (i.e., fly with level wings) during the mid-day hours when the solar energy capture of the SAIL aircraft would be improved. For example, for afternoons during which the SAIL aircraft's roll orientation is such that the wings are nearly orthogonal to the Sun, the aircraft are forced to fly level to improve solar energy capture. This is the only major change made to the guidance logic relative to the previous 30 day flight. Consequently, the net propulsion energy usage by DAP tends to be larger compared to the results provided in Figure 5 for which no attempt to improve mid-day solar energy capture is made.

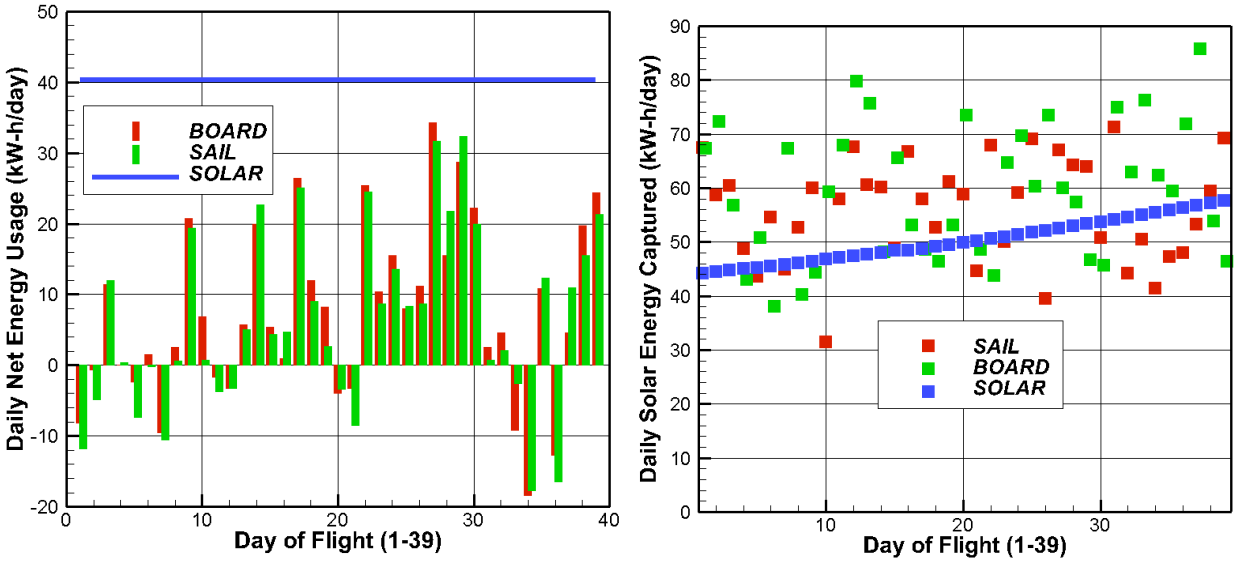


Figure 19. Daily energy usage and solar energy capture by DAP aircraft compared to pure solar aircraft over 39 days

Figure 19 (right) summarizes the solar energy capture for the SAIL and BOARD compared to the conventional SOLAR option. Although 20% efficient solar energy capture is assumed, the losses associated with storing/retrieving energy from the batteries, and converting the energy into usable propeller energy is reflected in the assumption here of an *effective* solar capture efficiency of 15%. Interestingly, because the DAP aircraft do not fly level, and use of solar film/cells on both upper and lower surfaces of the wings is useful, DAP captures more solar energy than the pure solar aircraft. Note that the DAP guidance software makes no attempt to improve solar energy input while sailing (i.e., orient the aircraft to improve solar capture), but such an approach could lead to more consistently large solar energy capture.

Figure 20 summarizes the daily net energy available to the payload (i.e., the solar energy input minus the propulsive energy usage) for the DAP (i.e., SAIL + BOARD) versus two SOLAR aircraft. This comparison assumes the SAIL and BOARD could transmit/share power along a thin electrical wire embedded within the cable. ***DAP consistently provides a great deal more energy to the payload than the two SOLAR aircraft.*** This comparison would become more stark near the winter solstice when available solar energy is at its minimum (i.e., one month

prior to this timeframe). From Figure 20 one could project that the pure solar aircraft would not be able to support a payload in the vicinity of that timeframe.

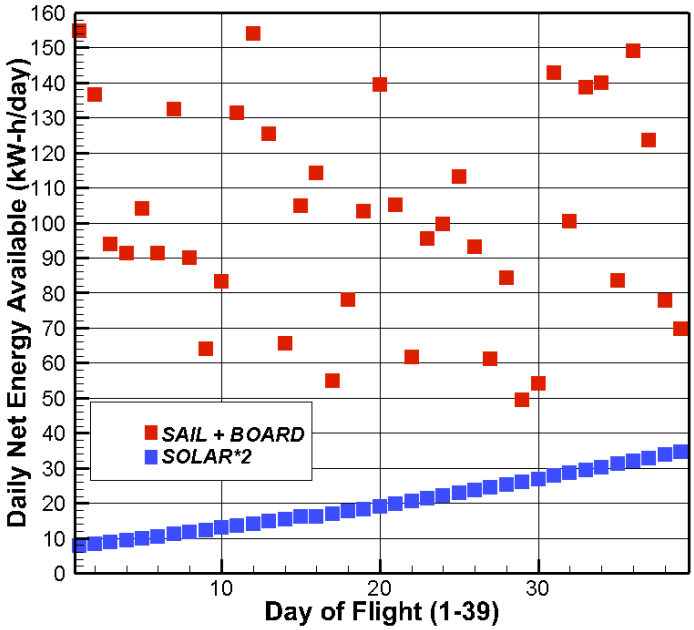


Figure 20. Daily net energy available to the payload by DAP aircraft compared to pure solar aircraft over 39 days in mid-late winter

### *5.4 DAP Trajectory Characteristics*

Figure 21 illustrates the altitude history (of SAIL aircraft), roll orientation for both SAIL and BOARD, and cable maximum tension, for one of the days (i.e., day #36) which produced negative net propulsive energy usage. In this case only a few significant altitude changes in the vicinity of 60,000 feet are made, and these coincide with nearly 180° turns made to remain within the 150-mile stationkeeping radius. The roll orientation of the SAIL is always less than that of the BOARD, as expected for sailing mode of flight. The orientations switch abruptly between positive and negative values each time the aircraft must make a turn. The ground track (not shown) involves back-and-forth flight at horizontal heading angles of approximately 45° and 225° from due north, respectively, throughout the day. The cable tension averages about 650 lbf and doesn't reach low tension except in the turns, which are omitted from the flight simulations. The cable tension is seen to resonate occasionally (e.g., between 10am and 11am) apparently due to interaction of the cable dynamics and turbine response, and can be addressed by improvements to the controls logic. Further dissemination and discussion of typical flight trajectories produced in these simulations is warranted, and will be provided in a future publication.

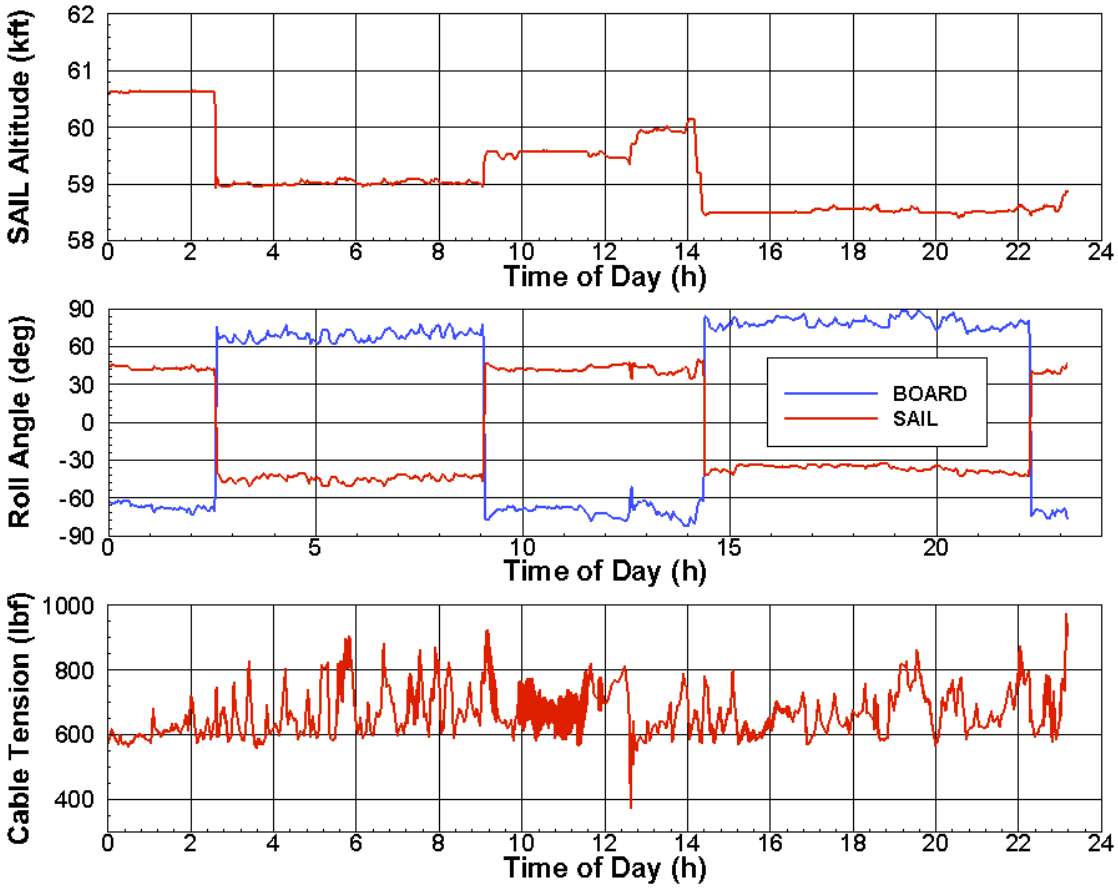


Figure 21. Trajectory altitude, roll orientation, cable tension histories for one day of flight

# 6.0 Communications Payload Design and Analysis

The main mission payload for DAP is a communications payload providing 700 MHz wireless data services to a region within 240 km of the city of Orlando, FL. Operating like a high-altitude, meandering cellular tower, DAP satisfies a wide-area-coverage role unattainable by fixed cellular towers, and at the same time comparing favorably to spacecraft solutions (e.g., Iridium). Example differences include:

- **Cellular:** About 3 km separation between towers; the DAP service region alone includes around 3500 discrete cellular towers. Each offers a high data capacity to a large number of users.
- **Iridium:** Just 66 spacecraft service the entire globe. A typical cell (spot beam) is about 488 km across (the size of the DAP coverage area) and serves about 80 simultaneous outdoor calls.
- **DAP:** One payload services 128 sliver-shaped cells and about 3,500 simultaneous indoor and outdoor calls within the 480 km service region; exact values vary with assumptions.

Although it is difficult for any SWAP-constrained platform (like DAP) to compete favorably with cellular networks within their established domain (e.g., population centers where thousands of towers exist), the properties of DAP make the platform ideal for providing service in applications unfavorable to cellular networks and traditionally serviced by spacecraft. Examples include operation in locations that are rural or undeveloped, off-shore, or otherwise afflicted by events that cripple the local infrastructure.

## *6.1 Analysis Description*

This work considered the DAP payload as a basic communications system having both transmitting receiving roles, and uses classic analysis techniques [14,15]. The system design describes major elements of each role for both the payload and user; these affect the effective isotropic radiated power (EIRP, $P_t G_t$) for transmitters, and the receiver figure of merit ($G_r/T$).A standard radio link budget was used to predict the link signal to noise ratio (SNR) as

$$SNR = \frac{(P_t G_t)}{kB}\left(\frac{G_r}{T}\right) L_p \eta .$$

These variables are determined (or set) for DAP as

- Antenna Gains ($G_t$, $G_\gamma$) from the platform size
- Power per call, $P_t$, from available payload power
- Radio link path loss, $L_p$, found by simulation
- Receiver noise, $T$, as 300 K (includes radio & earth)
- Signal bandwidth $B$, as 12.2 kHz (AMR speech)
- Required SNR for a link as 8 dB for decoding
- Typical efficiencies & margins $\eta$ for the application

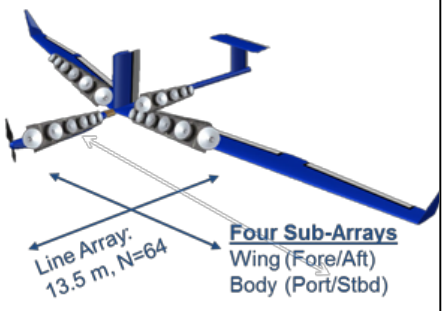

Figure 22. Conceptual antenna layout for DAP

*Antenna Description (Size Constraint)*

The antenna gains are constrained by the available surface area on DAP that can be used for antennas, and are assumed to be equal (the same antennas are used for both modes). Figure 222 shows the DAP approach in which the platform antennas are implemented as four distinct phased arrays of 64 discrete *elemental* antennas (wing fore/aft, and body port/starboard). The physical size of these arrays (13.5 m long, less than 21 cm tall) is based on the wavelength of the 700 MHz radio frequency used in this analysis. The elemental antennas are modeled as dual-polarized patches to support polarization diversity) having a gain of 4 dBi, for overall gains of about $G_t = G_\gamma = 22$ dBi. These arrays will be used to create 128 total sector beams, each covering about 2.8° of azimuth from DAP.

*Power*

The transmitted power per call, $P_t$, is constrained by the total available payload power, the number of simultaneous calls, and the means by which power is allocated to each call. Assuming that the total payload power $P_P$ is dominated by the transmitted power and the transmitter's efficiency $\varepsilon$, then the total power can be found by sum of the required power from all simultaneously-occurring calls as

$$P_P = \sum_n \varepsilon^{-1} P_{t,n} .$$

This work assumes a total payload power of 1 kW (constrained by the platform) and a transmitter efficiency of 40% (based on the Freescale Airfast AFT26HW050S/GS amplifier module). These choices yield 400 W to be distributed among all simultaneous calls.

*Radio Link Loss*

The loss on the radio link, $L_p$, is determined by the range, and terrain, between the DAP vehicle and the user, and varies for each prospective user location and the position of DAP within its flight path. This work simulated values of $L_p$ using the Irregular Terrain Model (ITM), in conjunction with 1-kilometer digital elevation maps (DEMs) of Florida. A simulation example is shown in Fig. 23a, assuming that the DAP vehicle is located at 60,000 feet at the the southern edge of the service region. This figure shows the range dependence of $L_p$ and also

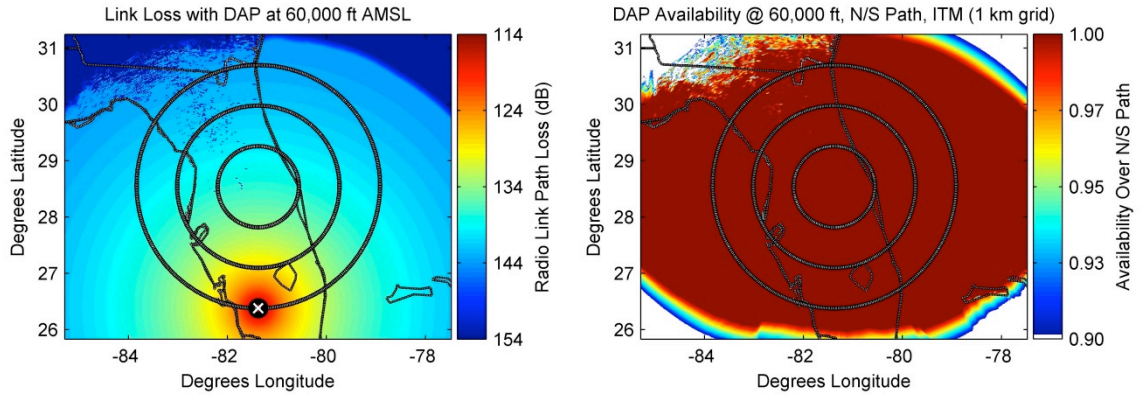


(a) (b)

Figure 13. (Left) Predicted radio link loss between DAP, located at 60,000 feet altitude at the 'x' location, and ground-level customers at locations throughout Florida. Isoranges from the Orlando city center are plotted at 80, 160, and 240 km. (Right) Analysis of the radio link availability showing that most positions within the service region are predicted to maintain line of sight to the DAP vehicle during a simplified north-south flight path.

identifies limited user locations at which the line to DAP is obstructed.

Locations without line of sight to DAP (dark blue in Fig. 23a) indicate potential users that will be unable to communicate with the payload, and are of special concern. Fig. 23b summarizes the results of an analysis of these locations, considered as the DAP traverses a simplified north-south flight path through the service region. The color indicates the predicted availability of the DAP service to each location, defined as the fraction of time for which line of sight (not shadowing) is predicted. While most points within the service region have a predicted availability near 100%, limited regions exhibit lower availabilities (95%) due to the local terrain. Future studies may refine these predictions using alternative radio models (such as AREPS, TEMPER, and PETOOL), as well as more-detailed DEMs.

*Noise, Bandwidth, and SNR*

The receiver noise, $T$ , signal bandwidth, $B$ , and minimum-required SNR, each contribute to the required sensitivity and achievable throughput of the DAP radio link. We adopt notional values for each of these quantities as-reasonable for the link:

- The receiver noise of 300 K includes estimated contributions of 150 K from the DAP antenna brightness temperature (which includes beams half-filled by the Earth) and 150 K from the electronics themselves (assuming low-noise receiver electronics).
- The signal bandwidth of 12.2 kHz is based on the assumption that the communications link will support the enhanced full rate (EFR) mode of adaptive multirate encoding (AMR) as specified for 3G cellular voice transmissions, assuming an overall spectral efficiency of 1 bps/Hz.
- The required SNR of 8 dB assumes that the radio link employs simple modulation (e.g., QPSK) and appropriate forward-error-correction encoding. While many different assumptions for link SNR are possible, and form the basis for selecting different encoding schemes for variable quality-of-service (QoS), such variations are outside the scope of this analysis.

*Typical Radio Link Margins*

The efficiencies and margins $\eta$ describe anticipated extra losses (beyond direct radio propagation), as well as the anticipated losses that must be anticipated by DAP when transmitting or receiving a signal. The major losses that were considered in this analysis include the following.

- **Antenna Pointing Loss** (3 dB), represents both combining inefficiencies in the DAP phased arrays (such as those caused by array windowing to lower the array sidelobes), as well as anticipated straddle losses (caused by users located in between the maxima for adjacent beams). This does not include loss due to the DAP platform orientation, which is considered later.
- **Handset Body Loss** (3 dB), caused by the user's interaction with the handset; this number is highly variable and selected as representative of values consistent with cellular link budgets.
- **Building Penetration Loss** (18 dB), selected as a typical value used in planning of 900 MHz GSM systems. This value is included only when considering users located inside buildings.
- **Uplink Excess Fading Margin** (10 dB), represents radio link losses caused by shadowing and multipath and not accounted for in the ITM simulation. This value is a representative worst-case for what is inherently a statistical phenomenon, and is selected

as consistent with cellular network planning. This is used to calculate the power requirement of the user's handset.

- **Downlink Excess Fading Margin** (0 dB total), represents the same phenomena as the uplink fading margin, but representing the average loss of 0 dB for the downlink (DAP to user). The average, rather than worst-case, is used to calculate the overall power requirements of the DAP payload when communicating with many users simultaneously.
- **Implementation Loss** (3 dB), as an estimate to encompass factors yet-unconsidered in this work.

*Handset Characteristics*

Key assumptions of the user handset, selected as-consistent with other analyses, include the following:

- **Handset antenna gain** (0 dBi), so that the user's gain is independent of orientation to DAP
- **Handset noise temperature** (1550 K), for low-cost receivers in a congested radio environment
- **Handset transmitter power** (2 W), found from the link budget for indoor users at the maximum range from DAP. This is consistent with modern mobile handsets.

*Anticipated Downlink Power*

At the maximum range of 480 km, analyses with the preceding values suggest that the DAP downlink will require about 17 mW of power per-user to serve outdoor users, and 1.1 W per-user for indoor users.

### *6.2 Average Users & Network Capacity*

As observed in Fig. 23, the radio link requirements are unique for customers at different locations relative to the DAP vehicle. Ultimately, the ability of DAP to serve multiple customers is constrained by the sum of the individual customer requirements in relation to the payloads maximum transmitted power (400 W). This aggregate is influenced, in turn, by four additional factors considered in the analysis.

- The geographical distribution of DAP customers, assumed to be uniform throughout the service region, representing rural users outside of traditional cellular coverage.
- The location of the DAP vehicle in relation to the center of the service region; vehicle locations near the edge of the service region will have higher maximum ranges to the furthest customers.
- The orientation (roll/pitch) of the DAP vehicle, and resulting implications on the projection of the antenna radiation patterns into the service region. The radiation pattern scanning loss is modeled to be consistent with that of the half-wave patch antennas composing the arrays.
- The split among indoor and outdoor users, which varies based on context (e.g., 6:1 in urban centers and 1:5 for rural areas); we adopt the 1:5 ratio anticipated for rural users.

*Simulation*

The location and orientation of the DAP platform affect the downlink power required for users at various positions throughout the service region. These effects were modeled in order to determine characteristics of the average user (e.g., the average downlink requirement across all

locations in the region). In addition to the link budget parameters as previously described, the model assumed a scan loss typical of half-wave patches for both the fore/aft and port/starboard arrays. The vehicle is assumed to use whichever array results in a more-favorable configuration.

Examples of two different states illustrating these effects are shown in Fig. 24. First, Fig. 24a represents the downlink power required as a function of user location assuming that the DAP vehicle is oriented level at the location indicated by 'x'; the required power varies with range, and exhibits a lobe structure consistent with switching between the fore/aft and port/starboard arrays. In contrast, Fig. 24b represents the required power when the DAP vehicle is located at the same location, but facing east with a 40° port roll. The starboard array (facing south) has been tilted up, requiring more power to users in those directions.

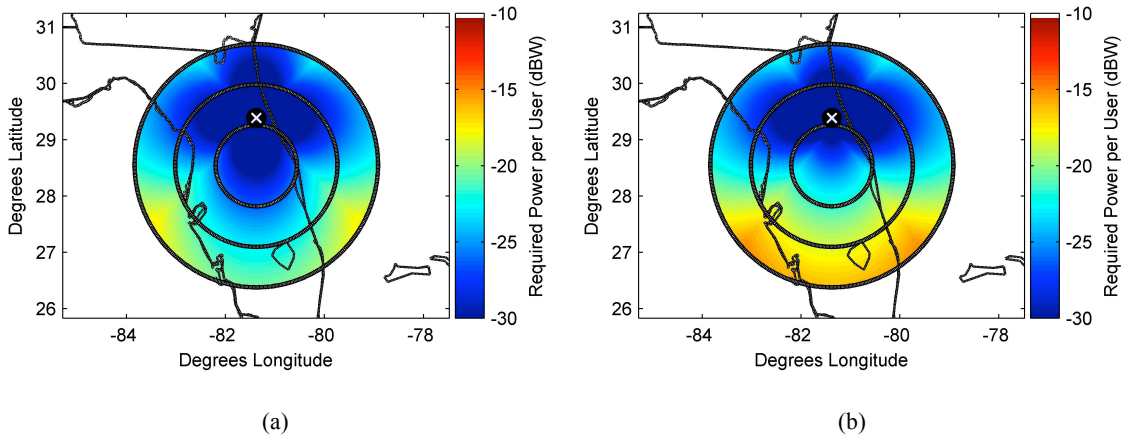


Figure 22. (Left) Required downlink transmitter power for outdoor users as a function of user location when DAP is located at the indicated position at 60,000 feet and in level orientation facing east. The lobe structure indicates transitions between the fore/aft and port/starboard arrays. (Right) The same except DAP is rolled by 40° to port, showing effect of scan loss.

*Determination of the Average User*

Results from analyses such as Fig. 24 can be used to determine the downlink power needed for the *average* DAP user, as a function of the DAP location and orientation, assuming that users are equally-likely to appear at any location within the service region. The results of such an analysis are shown in Fig. 25, and vary from about 3.5 mW per-user (DAP in level flight near the center of the region) to about 21 mW per user (DAP in a 40° roll at the edge of the service region). Approaches for mitigating the effects of this difference should be studied further, and might include:

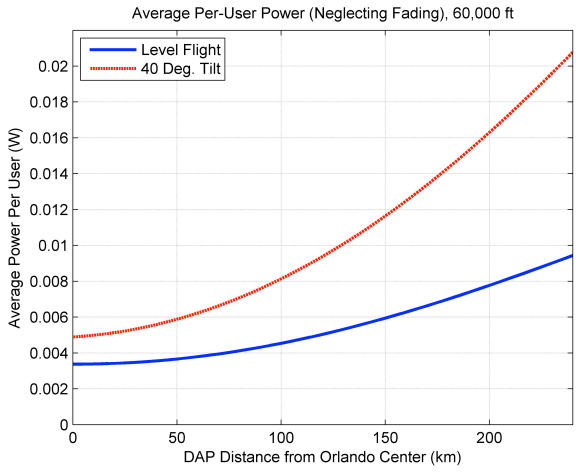


Figure 25. Aggregated results of downlink power required to the average outdoor user as a function of DAP location.

- Varying the total user capacity, while keeping the same quality of service (data rate) to each user.

- Varying the quality of service (e.g., through different AMR data rates), while keeping the total number of users constant; the AMR rates vary from 4.75 kbps to 12.2 kbps.
- Maintaining the same number of users and quality of service throughout the phases of flight, but varying the instantaneous payload power requirement (maintaining an average of 1 kW).
- Refining the elemental antenna design to permit compensation for the roll angle (e.g., electronic or mechanical steering along the roll axis to reduce scan loss).

*User & Subscriber Capacity*

The preceding analyses are used to predict the number of instantaneous users, and ultimately the number of subscribers, that might be supported by the DAP payload. Based on Fig. 2 and considering 400 W of available transmit power (from a 1 kW total payload power), the total number of simultaneous outdoor users is calculated by $P_{\mathrm{AV}} N_{\mathrm{out}} = 400\ \mathrm{W}$. Extending this to a mix of indoor and outdoor users, the total number of users is found by satisfying $P_{\mathrm{AV}} N_{\mathrm{out}} + G_{\mathrm{BPL}} P_{\mathrm{AV}} N_{\mathrm{in}} = 400\ \mathrm{W}$, where $N_{\mathrm{out}} = 5 N_{\mathrm{in}}$ is typical of a rural environment and $G_{\mathrm{BPL}} = 63.1$ to compensate for the building penetration loss. Finally, the number of supported *subscribers* is found by an assumption of a 15-30 mErl usage rate, which indicates that the typical call is between 54 s and 108 s. Using an average call power of 10 mW (based on level flight when DAP is 240 km from the city center), these expressions yield the following conclusions.

- **Number of Simultaneous Calls (Outdoor):** 40,000
- **Number of Simultaneous Calls (Rural 1:5 Mix):** 3,524
- **Number of Total Subscribers (Rural 1:5 Mix):** 117,470 to 234,930

Finally, the total spectrum allocation required for DAP is estimated by $2 \times 12.2\mathrm{kHz} \times N_{\mathrm{users}} 4/128 \times r^{-1}$. This first term, $2 \times 12.2\mathrm{kHz}$, indicates the spectrum requirement per-user for duplex audio. The middle term, $N_{\mathrm{users}} 4/128$, indicates the number of users in the busiest beam, assuming an even geographic distribution among DAP's 128 beams (when DAP is at the edge of the coverage region, the largest beam has 4 times the number of users vs. an even-split). Finally, the $r^{-1}$ term indicates that the allocated spectrum is increased by the spectral reuse rate, which we adopt as 0.5, to indicate that adjacent beams do not reuse the same radio channels. This leads to a required spectrum allocation of about 5.4 MHz for the rural mix of users; this is on-par with existing cellular band allocations.

# 7.0 Key Enabling Technologies

Before any stratospheric mission as a communications relay satellite could be realized, the new key technologies behind DAP operation must be matured and proven in flight. Starting from the highest-risk item, here are the top four key technologies identified from this study.

***#1. Development of flight software for autonomous guidance and control for all phases of flight after take-off, including the sailing mode of flight and related transition maneuvers.***

Technology item #1 contains the most risk because it is entirely unprecedented and is at the core of the DAP concept. The synergistic operation of two connected aircraft to permit sailing (and transitions between sailing and conventional flight) has been demonstrated by arguably realistic flight simulation in Phase I, leading to TRL of perhaps 3. However, successful flight demonstration using autonomous control is required to raise the TRL to 5. The required flight software should be further developed in a laboratory setting using hardware-in-the-loop, and then flight tested on one and then both DAP aircraft, in an incremental manner to reduce flight risk.

***#2. Development of miniaturized LiDAR wind profiler system to meet specifications on weight, power, range, and accuracy for stratospheric full-size DAP.***

Technology item #2 is expected to be achievable based on recent correspondence with LiDAR specialists at NASA Langley's Laser Remote Sensing Branch about implementation on DAP. LiDAR navigation systems have recently been drastically reduced in size and weight while improving performance, and a similar trend is expected for existing onboard LiDAR wind profiling systems. However, since DAP performance is strongly correlated with the performance of the LiDAR system, LiDAR development should be a relatively high priority.

***#3. Development of light, robust cable connection system that includes capability to retract/extend the cable between the aircraft.***

Technology item #3 is based on existing components (e.g., electric winches) but will require significant design effort to reduce weight and power usage, and to ensure reliable adjustment to the cable length for the long-duration DAP application. Also, the use of the aforementioned "roller-bearing" mechanism for cable attachment to the BOARD is novel and represents additional risk. Finally, the desire to measure cable tension and avoid any cable-to-aircraft impingement during transitions are also important considerations.

***#4. Development of efficient "turbine-mode" for the electrically-driven propeller propulsion unit to extract energy when encountering excessive shear and for intermittent descents.***

Technology item #4 has already been demonstrated by the Pipestral-Siemens WattsUP prototype. This prototype is a low altitude aircraft that uses the turbine mode for descent

only. It remains to be demonstrated that such a propulsion unit can be efficient in both propulsive and turbine modes for the high-altitude DAP application.

Flight simulation results indicate that, without this technology, DAP will still require substantially and consistently less energy for propulsion than a pure solar. So, item #3 doesn't appear to be required for a stratospheric DAP, and is deemed less critical than the previous items.

# 8.0 Conclusions

The DAP concept appears to be potentially viable alternative to the pure solar aircraft for the role of an atmospheric satellite, including as a communications relay over central Florida. Flight dynamics simulation using a detailed transient atmospheric model show that, with accurate LiDAR forecasting of wind profiles, the platform could remain in sailing mode for the vast majority of a long duration mission, greatly reducing the need for propulsion, compared to a pure solar aircraft. Additionally, the flight simulation results show that the SAIL and BOARD aircraft collects significantly more solar energy than the pure solar aircraft. The latter is related to the advantageous use of solar cells/film on both the upper and lower surfaces of the aircraft wings. Since no effort was made in the guidance software to improve solar capture while sailing, further development of the guidance software is expected to further improve solar energy capture. Finally, an evaluation of a baseline DAP communications package in the SAIL suggests that the changing roll orientation of the aircraft will require significantly more power to support communications compared to a pure solar aircraft, without a more complex antenna system or tighter stationkeeping radius.

## Acknowledgements

The PI would like to acknowledge the contributors to this report, including Dr. Hever Moncayo, Mr. Esteban Sanchez, and Mr. Agustin Giovagnoli from the ERAU Flight Dynamics and Controls Laboratory who supporting aircraft development and flight simulation efforts; Dr. Billy Barott from ERAU for development and analysis of the communications system; Mr. Ryan Decker from NASA MSFC for development of the long duration DRWP-based atmospheric models. We also would like to thank Boeing aircraft design experts, Mr. Norm Princen and Mr. Blaine Rawdon, and aerospace engineer, Mr. Kushan Patel, for volunteering their insight and support of the aircraft configuration efforts.

Finally, the PI would also like to thank the NASA Innovative Advanced Concepts (NIAC) program for providing the opportunity to develop the DAP concept.

# References


1. Engblom, W., *Development of Atmospheric Satellite Concept based on Sailing*, AIAA-2012-3203, Applied Aerodynamics Conference, AIAA-2014-1111, AIAA SciTech 2014, Jan 2014.
2. Engblom, W., *Dual-Aircraft Atmospheric Platform*, U.S. Patent Application No. 13/414,451, March 17, 2012.
3. Gentry, B., et al*, Flight Testing of the TWiLiTE Airborne Molecular Doppler Lidar,* International Laser Radiation Conference, St. Petersburg, Russia, Jul. 2010.
4. Kavaya, M., *The Doppler Aerosol Wind (DAWN) Airborne, Wind-Profiling Coherent-Detection Lidar System: Overview and Preliminary Flight Results*, Journal of Atmospheric and Oceanic Technology, 31.4, Apr 2014, 826-842.
5. Amzajerdian, F., Pierrottet, D., "Fiber-based Coherent Lidar for Target Ranging, Velocimetry, and Atmospheric Wind Sensing," Conference on Lasers and Electro-Optics; 21-26 May 2006; Long Beach.
6. Barbré, R. E. "Development of a Climatology of Vertically Complete Wind Profiles from Doppler Radar Wind Profiler Systems". 17th Conference on Aviation, Range, and Aerospace Meteorology. American Meteorological Society. Phoenix, Arizona. January, 2015.
7. Barbré, R. E., 2012: Quality control algorithms for the Kennedy Space Center 50-MHz Doppler radar wind profiler winds database. J. Atmos. Oceanic Technol., 29, 1731–1743.
8. Burns, K. L. "CCAFS RRA 2013 Development Report". Jacobs ESSSA Group Analysis Report. ESSSA-FY13-1655. February 19, 2013.
9. Spiekermann C. E., Sako B. H., and Kabe A. M. "Identifying Slowing Varying and Turbulent Wind Features for Day-of-Launch Flight Loads Analyses". 40th Structures, Structural Dynamics and Materials Conference, American Institute of Aeronautics and Astronautics. AIAA-99-1250. St. Louis, MO. April 1999.
10. Perez A., Moncayo H., Perhinschi M. G., Al Azzawi D., Togayev A., *A Bio-Inspired Adaptive Control Compensation System for an Aircraft Outside Bounds of Nominal Design*, Journal of Dynamic Systems, Measurement and Control, ASME, Vol. 137, Sep, 2015.
11. Moncayo, H., Krishnamoorty,K., Wilburn, B., Wilburn, J., Perhinschi , M., Lyons, B. *Performance Analysis of Fault Tolerant UAV Baseline Control Laws with L1 Adaptive Augmentation,* Journal of Modeling, Simulation, Identification, and Control, Columbia International Publishing, Vol.1, No.4, pp. 137-163, 2013.
12. Wilburn B., Perhinschi M. G., Moncayo H., Karas K., Davis J., *Unmanned Aerial Vehicle Trajectory Tracking Algorithms Comparison*, International Journal of Intelligent Unmanned Systems, Volume 1, Issue 3, 2013.
13. Perhinschi M. G., Wilburn B., Davis J., Moncayo H., Karas K., *Simulation Environment for UAV Fault Tolerant Autonomous Control Laws Development*, Journal of Modeling, Simulation, Identification, and Control, Columbia International Publishing, Vol.1, No.4, pp. 164-195, 2013.
14. Advanced Cellular Network Planning and Optimisation, A. R. Mishra (ed), Wiley, 2007.
15. 4G Deployment Strategies and Operational Implications, T. Krishnamurthy, R. Shetty, Apress, 2014